Biochemistry

pubs.acs.org/biochemistry Article

Allosteric Impact of the Variable Insert Loop in *Vaccinia* H1-Related (VHR) Phosphatase

Victor A. Beaumont, Krystle Reiss, Zexing Qu, Brandon Allen, Victor S. Batista,* and J. Patrick Loria*

Cite This: *Biochemistry* 2020, 59, 1896−1908 Read Online

ACCESS | Metrics & More | Article Recommendations | Supporting Information

ABSTRACT: Dynamics and conformational motions are important to the activity of enzymes, including protein tyrosine phosphatases. These motions often extend to regions outside the active site, called allosteric regions. In the tyrosine phosphatase *Vaccinia* H1-related (VHR) enzyme, we demonstrate the importance of the allosteric interaction between the variable insert region and the active-site loops in VHR. These studies include solution nuclear magnetic resonance, computation, steady-state, and rapid kinetic measurements. Overall, the data indicate concerted millisecond motions exist between the variable insert and the catalytic acid loop in wild-type (WT) VHR. The 150 ns computation studies show a flexible acid loop in WT VHR that opens during the simulation from its initial closed structure. Mutation of the variable insert residue, asparagine 74, to alanine results in a rigidification of the acid loop as observed by molecular dynamics simulations and a disruption of crucial active-site hydrogen bonds. Moreover, enzyme kinetic analysis shows a weakening of substrate affinity in the N74A mutant and a >2-fold decrease in substrate cleavage and hydrolysis rates. These data show that despite being nearly 20 Å from the active site, the variable insert region is linked to the acid loop by coupled millisecond motions, and that disruption of the communication between the variable insert and active site alters the normal catalytic function of VHR and perturbs the active-site environment.

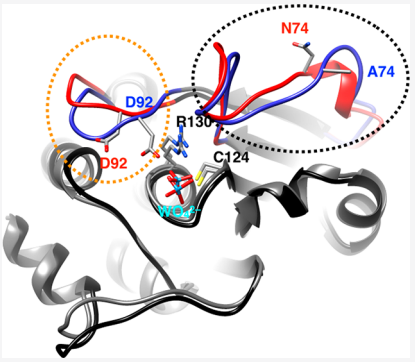

Protein tyrosine phosphatases (PTPs) are critical regulators of important biological processes;[1−4] *Vaccinia* H1-related (VHR) phosphatase (Uniprot entry 541452) is a 20 kDa PTP, and its catalytic activity is crucial for proper cellular function. VHR was initially classified as a dual-specificity phosphatase (DUSP), but later studies demonstrated a 10^3-fold preference for phosphotyrosine (pY)-containing substrates over phospho-Ser- or phospho-Thr-based substrates for VHR.[5,6] VHR is primarily a nuclear enzyme that acts on several different substrates, including STAT5 (signal transducers and activators of transcription),[7] MAP kinases ERK1 and ERK2,[5] JNK1 (c-Jun N-terminal kinase),[8] EGFR (epidermal growth factor receptor), and ErbB2.[9] In cervical cancer, VHR activity downregulates ERK1/2 and enhances cancer progression.[10] In addition, it was shown that siRNA silencing of VHR results in cell cycle arrest at the G1/S and G2/M stage.[11,12] Furthermore, in certain cell models of breast cancer[13] and non-small lung cell cancer cells,[9] the level of VHR expression decreases and upregulation of its expression slows cancer cell growth. These studies suggest that depending on the disease, inhibition or enhancement of VHR catalytic activity would be an avenue to therapeutic intervention.

Unfortunately, like all known class 1 PTPs, the high degree of active-site sequence conservation results in low specificity among competitive inhibitors, making them poor drug candidates. In addition, the necessity of a negatively charged ligand for binding to the highly conserved, electropositive active-site P-loop prevents such small molecules from crossing the cellular membrane as required for effective PTP inhibitors. These restrictive properties have resulted in PTP enzymes being dubbed undruggable.[14,15] However, allosteric ligands, which are not subject to the constraints of competitive inhibitors, represent a potential alternative.[16−18] There are a significant number of allosteric ligands described in the literature. Specific to phosphatases, some notable examples are the drugs cyclosporin and FK506 that target the Ser/Thr phosphatase, calcineurin.[19,20] Allosteric ligands have also been discovered to inhibit the PTP enzyme PTP1B.[21,22] Moreover, allosteric sites have been described for the Ser/Thr phosphatase, PP2A, that regulates its function,[23,24] and it has been shown that PDZ domains, which among their many functions, can convey allosteric ligand binding information via changes in dynamics, which may be important for the catalytic activity of protein tyrosine phosphatase 1E.[25,26] Recent work in our lab using a combination of mutagenesis and solution NMR spectroscopy has identified two allosteric sites in VHR.[27]

Received: March 26, 2020
Revised: April 29, 2020
Published: April 29, 2020

https://dx.doi.org/10.1021/acs.biochem.0c00245
Biochemistry 2020, 59, 1896−1908

However, an important next step is a mechanistic understanding of the linkage between the allosteric and active sites that results in alteration of catalytic activity.[14,28−30]

VHR shares a similar catalytic mechanism with the more thoroughly characterized PTP enzymes YopH and PTP1B (Figure 1A).[31,32] The enzyme active site is flanked by several

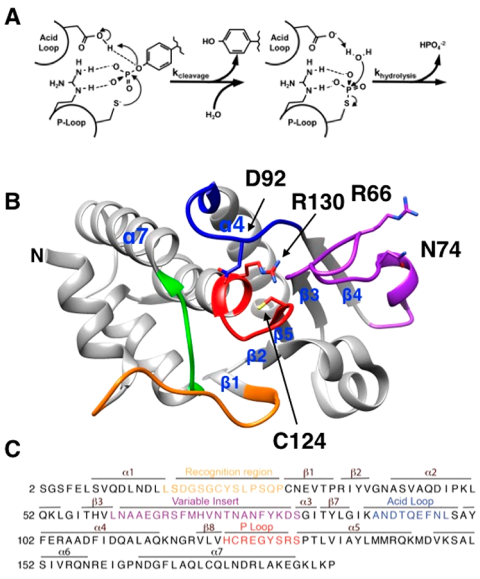

Figure 1. Mechanism and structure of VHR. (A) General mechanism of class I PTPs showing the cleavage step followed by the hydrolysis of the covalent intermediate. (B) Structure of VHR (PDB entry 1VHR) with the regions representing the recognition region (residues 19−29) colored orange, the variable insert (62−82) colored purple, the acid loop (89−99) colored blue, the P-loop (123−131) colored red, and the Q-loop (158−163) colored green. The catalytic acid D92, active-site nucleophile C124, P-loop residue R130, and allosteric residues R66 and N74 are represented as sticks. Selected secondary structure elements are labeled. (C) Primary sequence of VHR with relevant regions colored as in panel B.

loop regions, which are important for its function. The phosphate group from the substrate binds to the highly conserved P-loop (residues 123−131 in VHR). Additional binding interactions occur via the recognition loop (residues 19−29). Subsequent to substrate binding, PTP enzymes remove the phosphate group from tyrosine residues in two steps, cleavage and hydrolysis. Cleavage of the phosphotyrosine protein substrate occurs by nucleophilic attack from the conserved cysteine (C124) residue in the P-loop (Figure 1A,B). The phosphoenzyme intermediate is hydrolyzed in the second step to regenerate the active enzyme for the next catalytic cycle. Both steps involve the acid loop (residues 88−99) that contains a conserved aspartic acid (D92) located in the active site. In the cleavage reaction, D92 donates a proton to the leaving group tyrosine. By analogy with PTP1B and YopH, D92 also helps coordinate a water molecule for the subsequent hydrolysis step (Figure 1A).[6,31−36]

There are a few notable differences among VHR, YopH, and PTP1B with regard to the active-site loops. Crystal structures of apo and ligand-bound forms of both PTP1B and YopH show distinct open and closed conformations of the acid loop, respectively. In the loop-open conformation of these enzymes, the catalytic acid is ∼10 Å from where it needs to be to protonate the leaving group tyrosine.[34,37−41] Thus, loop closure is essential for catalysis, and in the closed conformation, the aspartic acid is brought into the proximity (∼4 Å) of the substrate for efficient protonation. In contrast, the X-ray structures of VHR show the acid loop to be in the closed conformation,[6,42] although there is no available structure of VHR with an empty active-site pocket. In the three published structures of VHR, the active site is occupied by the peptide substrate [Protein Data Bank (PDB) entry 1J4X], and the sulfonate moiety of HEPES buffer (PDB entry 1VHR) and a derivative of ethanesulfonic acid (PDB entry 3F81) are bound to the active site.[6,42,43] It is therefore uncertain whether VHR utilizes a flexible acid loop in its catalytic cycle. An additional differentiating feature from PTP1B and YopH is the presence of the so-called variable insert (VI) loop (residues 62−82), which connects β3 and β4, and this connecting region is significantly shorter than in YopH or PTP1B (Figure 1B,C). The VI has been suggested to be a site that facilitates VHR dimerization[44] and is the location of an allosteric site that has been identified by solution NMR methods.[27]

Here, we provide results of initial NMR experiments on wild-type (WT) VHR and further examine the role of the variable insert by mutation of a central residue in this region, N74, followed by characterization by solution NMR spectroscopy, computation, and enzyme kinetic assays. N74 is 12.4 Å (Figure 1B) from the catalytic cysteine nucleophile yet alters aspects of VHR catalytic activity, ligand binding, and proteinwide NMR chemical shifts and molecular motions, further bolstering the VI as an allosteric site in VHR.

MATERIALS AND METHODS

Site-Directed Mutagenesis. Mutants of VHR were prepared by polymerase chain reaction using oligonucleotide primers purchased from Keck Biotechnology Resource Laboratory (Yale University), and DNA sequences were confirmed by DNA sequencing performed by the Keck Biotechnology Resource Laboratory. The following sequences of the mutagenic primers were used: 5′-GTCCTTGTAGAAGTTGGCAGCGGTGTTGACGTGCATGAAG-3′ and 5′-TTCATGCACGTCAACACCGCTGCCAACTTCTACAAGGAC-3′ for N74A and 5′-GCCTAGTTTCTGCAGCGCGGGGATGTCCTGAGCC-3′ and 5′-GGCTCAGGACATCCCCGCGCTGCAGAAACTAGGC-3′ for K50A.

Protein Expression and Purification. VHR was expressed and purified as previously described.[27] The gene sequence for VHR contains a polyHis tag preceding a TEV cleavage site at the N-terminus. The DNA for this protein construct in plasmid pet43.1b was transformed and expressed in *Escherichia coli* BL21 (DE3) cells in either LB (for kinetic studies) or M9 (for NMR studies) minimal medium in the presence of 100 mg/mL carbenicillin. Expression started with a 10 mL culture of cells in LB placed in a 37 °C incubator being shaken at ∼180 rpm overnight. Inoculation of 1 mL of this culture into either 500 mL of LB or 25 mL of 50% D_2O M9 minimal medium and placed back in the incubator. Minimal medium cultures were incubated for 8 h before inoculation of 5 mL into 50 mL of 100% D_2O M9 minimal medium and shaken at 37 °C overnight. This culture was then inoculated into 1 L of 100% D_2O M9 minimal medium supplemented with $^{15}NH_4Cl$ and [^{13}C]glucose (when necessary) and placed back in the incubator. All *E. coli* cultures for protein expression were induced with 1 mM IPTG once the OD_{600} reached ∼0.8, at which point the cultures were placed in a 25 °C incubator rotating at 200 rpm for 16−18 h. For selectively reverse-

https://dx.doi.org/10.1021/acs.biochem.0c00245
Biochemistry 2020, 59, 1896−1908

labeled samples, 500 mg/L amino acids of natural isotope abundance were added to the minimal medium cultures 15−45 min prior to induction, following previously published procedures.[45] Eleven ^{2}H-, ^{13}C-, and ^{15}N-labeled samples supplemented with an individual isotopically natural abundance amino acid (Ala, Arg, Asn, Gln, Gly, Lys, Met, Phe, Ser, Thr, or Tyr) and two samples supplemented with nine (Ala, His, Leu, Lys, Ile, Met, Arg, Ser, or Val) and three (Ile, Leu, or Val) different amino acids were prepared using this method. Cells were harvested by centrifugation at 7000 rpm for 45 min and stored at −80 °C.

Purification of VHR started by resuspending cells in ∼15−18 mL of lysis buffer [20 mM Tris base, 500 mM NaCl, 20 mM imidazole, 5 mM 2-mercaptoethanol, and 5% glycerol (pH 7.4)] and lysed by sonication (3 s on/off for a total on time of 2 min at 75% amplitude). The lysate was clarified by centrifugation at 13000 rpm for 45 min and filtered through a 0.45 μm filter. The filtered lysate was then added to 5 mL of NTA-Ni resin and nutated for ∼1 h. The resin was washed with 75 mL of lysis buffer, and VHR was subsequently eluted with 50 mL of elution buffer [20 mM Tris base, 500 mM NaCl, 500 mM imidazole, 5 mM 2-mercaptoethanol, and 5% glycerol (pH 7.4)]. The purity of the collected fractions was verified by polyacrylamide gel electrophoresis (PAGE) before dialysis into lysis buffer for >4 h at 4 °C with a 1:20 TEV/VHR mixture. The fractions were added to another column with NTA-Ni resin using an identical protocol. The purities of collected fractions of VHR were again verified by PAGE and dialyzed into either kinetic buffer [100 mM NaAc, 50 mM Bis-Tris, and 50 mM Tris (pH 5.5)] or NMR buffer [20 mM Bis-Tris propane, 100 mM NaCl, 1 mM TCEP, 1 mM EDTA, 7% D_2O, and 2% NaN_3 (pH 6.5)]. The concentration of VHR was determined using the extinction coefficient at 280 nm of 11500 M^{-1} cm^{-1}.

Kinetic Assays. Steady-state kinetics were measured at 25 °C for WT VHR, N74A, and K50A with *p*-nitrophenyl phosphate (pNPP) at several concentrations (0.1, 0.2, 0.4, 0.6, 0.8, 1, 2, 4, 8, 10, 12, and 20 mM) following a previously published protocol.[46] Enzymes and pNPP were prepared in kinetic buffer, and the reaction was quenched with 1 M NaOH 10, 20, 30, and 40 s after the addition of the enzyme to PNPP. The rate was determined by the slope of the absorbance at 405 nm using the extinction coefficient of PNP (18000 M^{-1} cm^{-1}) as a function of time. The enzyme concentration-adjusted rate as a function of pNPP concentration was measured in triplicate and fit with the Michaelis−Menten equation in GraphPad Prism version 7 for MacOS X. Michaelis−Menten plots of WT, K50A, and N74A are provided in Figure S1A.

Transient kinetic assays were performed according to published methods with WT VHR, K50A, and N74A, at 25 °C using a 100 mM sample of pNPP in kinetic buffer on an SX20 stopped-flow instrument (Applied Photophysics).[46] The absorbance at 400 nm was recorded over time (≤1 s), and the concentration of *p*-nitrophenolate (PNP) determined by the experimentally measured extinction coefficient (847 M^{-1} cm^{-1}). Rapid kinetic data for five separate mixing events were averaged. The change in concentration of PNP versus time was fit with the following equation:

$$[\mathrm{PNP}] = ae^{-kt} + bt + c$$

where a is the burst size and proportional to the concentration of the enzyme, k is the sum of the rate of cleavage ($k_{cleavage}$) and the rate of hydrolysis ($k_{hydrolysis}$), and b is equal to $k_{cleavage}k_{hydrolysis}/(k_{cleavage} + k_{hydrolysis})$. Measurements of the concentration of PNP as a function of time as a result of cleavage of pNPP by WT, K50A, and N74A are shown in Figure S1B.

Nuclear Magnetic Resonance Spectroscopy. All NMR experiments were performed on a 600, 700, or 800 MHz Varian spectrometer at 25 °C. The standard triple-resonance experiments, including HNCA, HN(CA)CB, HN(CA)CO, HN(CO)CA, HN(COCA)CB, and HNCO, were performed for resonance assignments. The assignment process was facilitated by the Computer-Aided Resonance Assignment (CARA, cara.NMR.ch) and SPARKY software packages.[47,48] To further aid the assignment process, HSQC and two-dimensional (2D) HN(CO) spectra were recorded for each sample of 13 different selectively reverse-labeled amino acid VHR samples. The spectra from these samples were then compared to the same spectra from a uniformly ^{2}H-, ^{13}C-, and ^{15}N-labeled sample. The resonance assignments have been deposited in the BioMagResBank (BMRB) as accession number 27950.

The titration of phosphate to VHR was performed by preparing a 1.8 M solution of Na_2HPO_4/NaH_2PO_4 (pH 6.5) in NMR buffer and adding small aliquots (<5 μL) to the enzyme sample until saturation ($[PO_4]/[VHR]$ = 84 for WT VHR). An HSQC spectrum was collected after each addition of the solution to the sample to track the chemical shift differences and to determine the saturation point. VHR saturation with phosphate was assessed when additional titrations yielded no further change in the chemical shift. The tungstate titration was performed in an analogous manner with a 50 mM solution of Na_2WO_4 and larger aliquots (≤10 μL). Saturation for WT VHR was achieved when $[WO_4]/[VHR]$ = 5. The composite chemical shift differences ($\Delta\delta$) were calculated as previously published:[49]

$$\Delta\delta = \sqrt{\left(\delta_{\mathrm{H}}^{\mathrm{apo}} - \delta_{\mathrm{H}}^{\mathrm{bound}} + \frac{\delta_{\mathrm{N}}^{\mathrm{apo}} - \delta_{\mathrm{N}}^{\mathrm{bound}}}{25}\right)^2}$$

where δ_H and δ_N are the ^{1}H and ^{15}N chemical shifts and δ^{apo} and δ^{bound} are the chemical shifts of the apo and bound forms, respectively.

^{15}N CPMG relaxation dispersion experiments were performed on a 700 μM ^{2}H- and ^{15}N-labeled VHR sample using 32 scans per 128 t_1 increments. The ^{1}H carrier frequency was set to the water resonance with the ^{15}N carrier set to 120 ppm. Spectral widths in the ^{1}H and ^{15}N dimensions were 15 and 44 ppm, respectively. The ^{15}N CPMG relaxation dispersion experiments were performed at 600, 700, and 800 MHz with the spin−echo pulse train delay (t_{cp}) set to 0.5, 0.625, 0.7143, 1.0, 1.25, 1.667, 2.0, 2.5, 3.333, 5.0, 10.0, and 20.0 ms in the relaxation-compensated experiment.[50] A constant relaxation time of 40 ms was used for each.[51] The apparent transverse relaxation rate constant ($R_{2,app}$) was determined using the in-house software. The $R_{2,app}$ values were then fit to the Carver−Richards equation[52] using Mathematica version 12.1 Student Edition for MacOS X.

The TROSY Hahn-echo experiment[53] was performed on either 700 or 965 μM VHR with identical spectral parameters except the number of acquisitions was 72, 72, and 576 for the α, zz, and β experiments, respectively. The Hahn-echo experiments were performed on apo WT, WO_4-bound WT, and WO_4-bound N74A with a relaxation delay time of 48.6 ms

https://dx.doi.org/10.1021/acs.biochem.0c00245
Biochemistry 2020, 59, 1896−1908

to obtain information about millisecond time scale motions.[53] The experiment was collected in three separate spectra corresponding to the experiments measuring the transverse relaxation rate constants for the narrow (R_2^{α}) and broad (R_2^{β}) ^{15}NH doublet components as well as the relaxation rate constant for the longitudinal two-spin order ($R_1^{2\,HzNz} \approx R_1^{H} + R_1^{N}$), which are termed the α, β, and zz experiments. The β experiment is inherently weak in signal to noise; therefore, the number of acquisition scans was significantly increased relative to those of the other two experiments. The ratios of the signal intensities and the calculated R_{ex} values were determined for each well-resolved resonance with sufficient signal to noise as previously described.[53]

Computational Studies. Molecular dynamics simulations were performed on WT VHR (PDB entry 1VHR[6]) and two mutants (N74A and K50A). Tungstate was placed in the P-loop active site, in line with experimental conditions and reported crystallographic structures of other small molecules (e.g., phosphate) bound to VHR. Simulations were conducted in a periodic water box for 150 ns using the CHARMM36[54] force field and NAMD package.[55] The water box, including 150 mM NaCl, was created by adding water for 15 Å in the positive and negative x, y, and z directions around the protein, yielding a rectangular box with dimensions of ~72 Å × 65 Å × 82 Å. Long range interactions were handled using the default particle mesh Ewald electrostatics algorithm. Default X-PLOR-type van der Waals switching and electrostatic shifting functions were used, with a cutoff of 12 Å and a switching distance of 10 Å.

Before the production run was performed, the systems were minimized for 100 steps using a conjugate gradient algorithm and then gradually heated using a Langevin thermostat to 310 K three times. First, only the water and ions were minimized and heated. Next, the protein side chains were released to be minimized and heated with the solvent in an identical manner. To heat, the temperature was increased by 10 K at a time, equilibrated for one hundred 2 fs time steps (0.2 ps), and increased again until the temperature reached 310 K. The system was then equilibrated for 50 ps. Finally, the entire system was minimized and heated together. When the entire system was heated, the temperature step size was decreased to 1 K and the system was equilibrated at 310 K for 100 ps before initializing the production run. Postsimulation analyses were performed using VMD[56] [hydrogen bond and root-mean-square deviation (RMSD) analyses]. Hydrogen bonds were defined by a heavy atom distance of <3 Å and an acceptor−donor−hydrogen angle of <30°. Mutants were created in silico and energy minimized using the three-phase method described above prior to production MD runs.

RESULTS

NMR Backbone Assignments. VHR is a 185-amino acid residue (20.5 kDa) enzyme. Despite its modest size, by solution NMR standards, the resonance assignment process proved to be exceptionally difficult. This difficulty was due to resonance overlap and missing connectivities between a number of amino acids in the triple-resonance experiments due to low peak intensity. Therefore, in addition to acquisition of the standard backbone assignment experiments, TROSY-based HNCA, HNCACB, HNCACO, HNCOCA, HNCO-CACB, and HNCO experiments were performed.[57,58] We also performed a number of amino acid-selective reverse-labeling experiments according to published methods[45] to overcome these assignment problems. Eleven different samples of ^{2}H-, ^{13}C-, and ^{15}N-labeled VHR were prepared, each with a different naturally abundant ^{1}H-, ^{12}C-, and ^{14}N-labeled amino acid (alanine, arginine, asparagine, glutamine, glycine, lysine, methionine, phenylalanine, serine, threonine, or tyrosine). The HSQC and 2D HN(CO) spectra of these samples were compared to the spectra of a uniformly ^{2}H-, ^{13}C-, and ^{15}N-labeled VHR sample. Two combinatorial reverse-labeled samples were also prepared in which one sample was reverse-labeled with natural abundant isotopic versions of alanine, histidine, isoleucine, leucine, valine, lysine, methionine, arginine, serine, glycine, and cysteine and a separate sample with added isoleucine, leucine, and valine. The former sample further decreased the spectral overlap and isolated the resonances in the acid loop. The latter sample was prepared because isoleucine, leucine, and valine are metabolically scrambled in *E. coli* and could not be prepared separately.[47] The reverse-labeling protocol resulted in 14 additional assignments as well as confirmation of assignments obtained by standard triple-resonance experiments. This combination of methods results in a total of 158 of 178 non-proline assignments.

At this stage, many of the unassigned resonances were located in the loop regions (VI loop, P-loop, and Q-loop), which suggested that they were exchange broadened due to molecular motion. To overcome this problem, we produced two isotopically (^{2}H, ^{13}C, and ^{15}N) labeled VHR samples in which we titrated either inorganic phosphate or sodium tungstate, reaction product mimics, into the active site. Upon binding to these ligands, several additional resonances became resolved in the 2D ^{1}H−^{15}N HSQC spectrum. The signal to noise of these additional peaks was sufficient such that they could be assigned using HNCA and HNCACB experiments. The residues assigned in this fashion were G65, V71, N74, I83, A90, D92, T93, N97, Y128, and R130. Using these complementary approaches, we assigned a total of 93% (166 of 178 non-proline residues) of the VHR backbone. These assignments have been deposited in BMRB entry 27950.[59]

Ligand Titrations Suggest Allosteric Sites in Wild-Type VHR. In the process of the PO_4^{3-} and WO_4^{2-} titrations, we noticed chemical shift changes distant from the VHR active site. Even though the ligand titrations were intended to aid in the assignment process, the global response of VHR to binding of these anions was informative with respect to the allosteric network throughout the enzyme.[60] The composite chemical shift differences ($\Delta\delta$) relative to the apoenzyme as a function of the residue number show which residues are significantly perturbed to values greater than 2σ above the 10% trimmed mean (Figure 2 and Figure S2). As expected, the largest perturbations were detected in the acid loop (residues 89−99), P-loop (residues 123−131), and Q-loop (residues 158−163), where direct interactions with these oxyanions occur. In these regions, A90, T93, E95, F96, L98, C124, R158, E159, and G161 have elevated $\Delta\delta$ values in the phosphate titration and K89, D92, E95, F96, L98, H123, C124, R158, E159, and G161 have elevated values in the tungstate titration. However, significantly elevated $\Delta\delta$ values were also observed in the previously identified allosteric sites[27] in the variable insert (A62, A63, and V71 for both ligands and N74 only with tungstate). Residues in the α4−α7 region (A100, D164, G165, F166, L167, and A168 with phosphate and G165, F166, and L167 with tungstate) also had elevated $\Delta\delta$ values. Other residues with significantly large $\Delta\delta$ values include residues in

https://dx.doi.org/10.1021/acs.biochem.0c00245
Biochemistry 2020, 59, 1896−1908

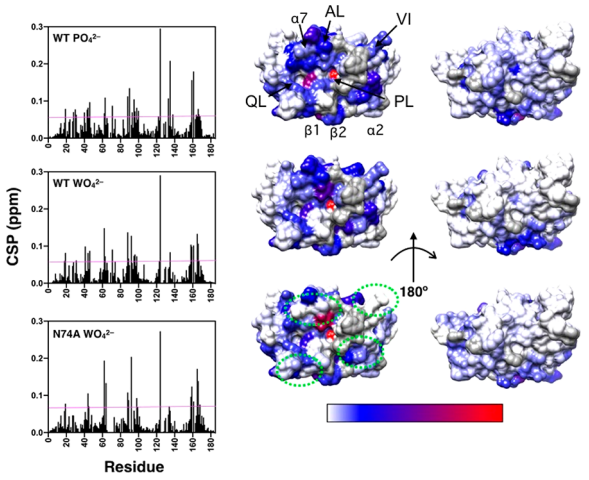

Figure 2. Ligand-induced chemical shift perturbations (CSPs). The left panel shows CSP values vs amino acid residue for WT and N74A with the respective complexes indicated in each graph. The magenta line represents 2σ above the 10% trimmed mean value for all three data sets. The right panels show CSP values mapped onto a surface rendering of VHR shown in the same orientation as in Figure 1B. CSP values above the magenta line are mapped according to magnitude (shown in the bottom bar) ranging from blue to red. Residues with CSP below this threshold are colored white. Residues that are unassigned, prolines, or have poor signal to noise that precludes measurement are colored gray. Regions that show significant differences from WT in the tungstate-bound complex are enclosed in green dashes. The acid loop (AL), P-loop (PL), Q-loop (QL), variable insert (VI), and select secondary structure elements are denoted in the top structure.

the recognition region (G19 and Q28), β1 (C30 and N31), β2 (G40), α2 (S43 and V44), β5 (V122), α5 (T133, V135, and Y138), and Q46 and I88 with phosphate and D18, G19, N31, (β2) N41, V44, Q46, I88, and V135 with tungstate. There are also subtle differences in the CSP patterns between phosphate- and tungstate-bound WT complexes that are suggestive of ligand-dependent allosteric differences in VHR. Overall, these titration data indicate that the anion binding to the P-loop of VHR propagates to the distal regions of the enzyme, including the VI and α7, and is consistent with the previous studies that identified these regions as allosteric in VHR.

Millisecond Motions Link the VI and Acid Loop in VHR. Some PTP family members possess a mobile acid loop,[61−63] whereas in other family members such as VHZ, the acid loop appears to be immobile.[64] To investigate whether the acid loop or other regions of apo VHR are flexible, we performed ^{15}N Carr−Purcell−Meiboom−Gill (CPMG) relaxation dispersion experiments to assess the dynamics on the millisecond time scale. The apparent transverse relaxation rates (R_2) as a function of the pulsing frequency ($1/t_{cp}$) in the CPMG spin−echo pulse train were measured, and the two-site Carver−Richards equation[52] was fit to the relaxation data obtained at three different static magnetic fields (600, 700, and 800 MHz). A global fit[65] of the relaxation data for the acid loop, including residues K89, D92, E95, F96, L98, and S99, yielded rates of exchange (k_{ex}) of 1400 ± 200 s^{-1}, a population of the major conformation (p_A) of 98.9 ± 0.1%, and residue-specific ^{15}N chemical shift differences between the major (conformation A) and minor (conformation B) conformations [$\Delta\omega_N = |\omega_N(A) - \omega_N(B)|$] of 1040 ± 96, 840 ± 175, 1800 ± 400, 1170 ± 147, 1790 ± 321, and 700 ± 97 s^{-1}. The Akaike information criterion (AIC) for this fit is 1014, and an F-test

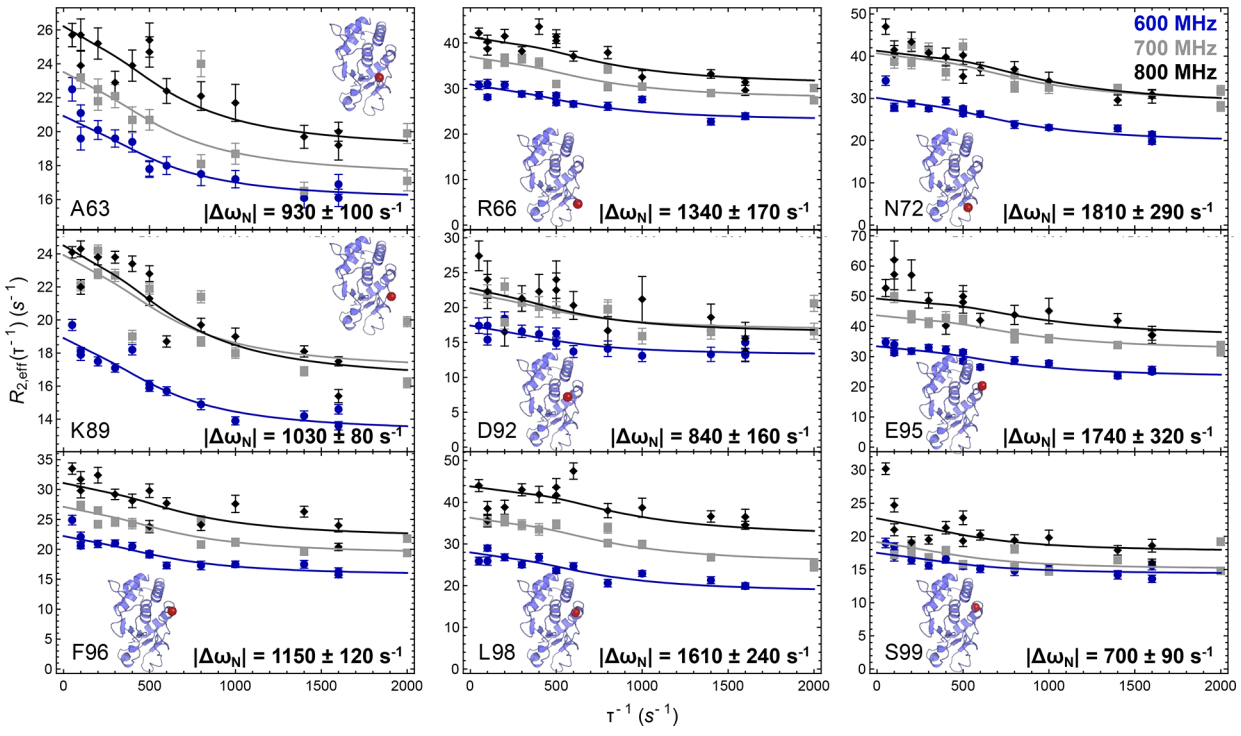

Figure 3. Millisecond motions in VHR. ^{15}N CPMG relaxation dispersion curves for residues A63, R66, N72, K89, D92, E95, F96, L98, and S99. The blue circles, gray squares, and black diamonds correspond to data collected at 600, 700, and 800 MHz, respectively. The insets show the crystal structure of VHR with the location of the corresponding residue represented as a red sphere. The curves represent a global fit to all nine data sets at three static magnetic field strengths. $\Delta\omega$ values are given at the bottom of each graph.

https://dx.doi.org/10.1021/acs.biochem.0c00245
Biochemistry 2020, 59, 1896−1908

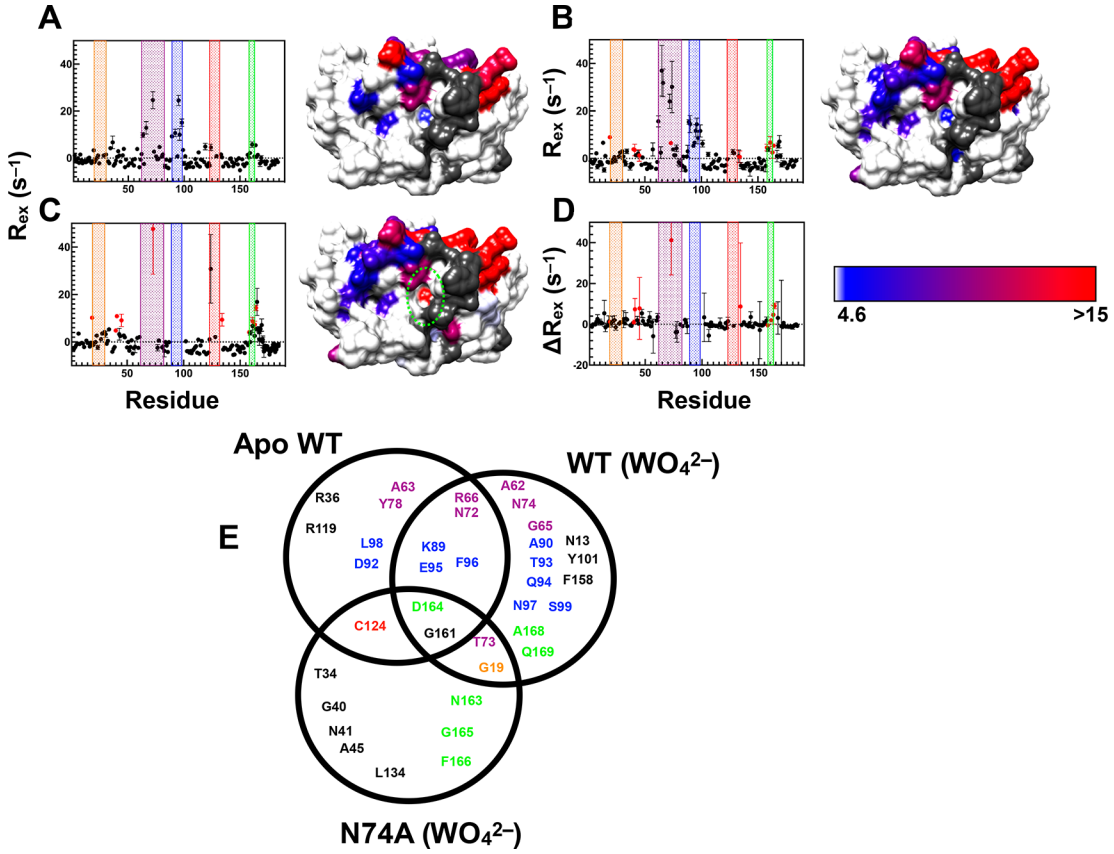

Figure 4. Millisecond motions in VHR. Residues with elevated R_{ex} values as determined by Hahn-echo measurements are graphed vs amino acid sequence and mapped onto the surface rendering of WT VHR in the (A) apo and (B) tungstate-bound complexes. In panel C, residues with elevated R_{ex} values in the tungstate-bound form of N74A are shown. In panel D, the difference in R_{ex} between tungstate-bound WT and tungstate-bound N74A (N74A − WT) is shown vs residue number. Residues with R_{ex} values below the 10% trimmed mean + 2σ (i.e., 4.6 s^{-1}) are colored white. Residues with R_{ex} values greater than this threshold are colored from blue to red according to the color key located at the bottom left. Regions in gray represent unassigned, proline, or overlapped residues, as well as residues with insufficient signal to noise. In each graph, as in Figure 1, the recognition region, VI, acid loop, P-loop, and Q-loop are colored orange, purple, blue, red, and green, respectively. Regions with different millisecond motions from the respective WT complex are enclosed within green dashes. (E) Venn diagram showing residues with elevated R_{ex} values from the NMR Hahn-echo experiment for apo WT and tungstate-bound WT and N74A. Residues are color-coded according to the color scheme in Figures 1 and 4. The VHR orientation of the VHR structure in panels A−C is identical to that in Figures 1 and 2.

comparison yielded a p value favoring the global model of 1.08 × 10^{-9} in which all residues share k_{ex} and population values.

These NMR relaxation experiments also revealed that the allosteric VI region exhibited considerable millisecond motions. A global fit for residues A63, R66, and N72 in VI yielded similar fit values as obtained for the acid loop with a k_{ex} of 2100 ± 460 s^{-1}, a p_A of 98.5 ± 0.4%, $|\Delta\omega_N|$ values of 920 ± 150, 1240 ± 230, and 1580 ± 360 s^{-1}, a global AIC of 457, and a p value of 1.38 × 10^{-5}. Considering the similarities in the kinetics and populations for both the acid loop and variable insert, we attempted to fit both regions to a single-global conformational exchange process (Figure 3). This global fit yielded a k_{ex} of 1530 ± 200 s^{-1} and a p_A of 98.8 ± 0.1% and statistical parameters with a p value of 8.2 × 10^{-14} and an AIC of 1478 for the global model versus fitting the two regions separately. The global $|\Delta\omega_N|$ values for A63, R66, N72, K89, D92, E95, F96, L98, and S99 for this fit are 930 ± 100, 1340 ± 170, 1810 ± 290, 1030 ± 80, 840 ± 160, 1740 ± 320, 1150 ± 120, 1610 ± 240, and 700 ± 90 s^{-1}, respectively and are also shown in the bottom of each panel of Figure 3. The global fit for all residues is shown in Figure 3. Improving the error of the fit and the model test parameters suggests that these two regions are likely involved in a concerted motion on the millisecond time scale.

Mutation in the Variable Insert Allosteric Site. On the basis of the chemical shift perturbation data with tungstate and phosphate and the NMR relaxation experiments that together suggest an allosteric interaction and concerted motions between the VI and active-site acid loop, we examined the effect of mutation of N74 to alanine. The N74A mutation is located in the VI loop and was previously identified as allosterically linked to the active-site acid loop and was therefore a logical first choice to address this issue. At its closest, N74 is 16 Å from C124, the active-site nucleophile, and the side chain of N74 is solvent-exposed. This alanine point mutation does not significantly perturb the overall fold of VHR as evidenced by the similarities in the HSQC spectra between WT and N74A that resulted in the small magnitude of the $\Delta\delta$ relative to WT (<0.2 ppm) (Figure S2). However, it is worth noting that several residues, mostly in the active site and VI, in the N74A mutant were broadened beyond detection in the apoenzyme of N74A, suggesting an enhancement of millisecond motions caused by mutation of this residue. Specifically, R66, V71, N72, I88, A90, D92, A100, R130, and G161 were broadened in the apo spectrum of N74A. Of these

https://dx.doi.org/10.1021/acs.biochem.0c00245
Biochemistry 2020, 59, 1896−1908

residues, those not in VI such as I88, A90, D92, A100, R130, and G161 are all >10 Å from N74. This indicates that the effect of mutation is propagated beyond the local region of N74, reinforcing the allosteric impact of this residue and the close linkage between VI and the acid loop and active site (Figure 2).

As with the WT enzyme, a tungstate titration was performed with N74A to assess the response of this variant to binding of the product analogue. The tungstate titration with N74A reveals 19 residues with elevated $\Delta\delta$ values. Seven of these residues are located in the active site (K89, E95, L98, S99, C124, R158, and E159), and five in the allosteric sites (A62, E64, G165, F166, and A168). Other residues with elevated $\Delta\delta$ values include D18, G19, N41, V44, A45, and L134. In addition, V71, I88, A90, D92, Q94, A100, R130, and G161 could not be analyzed due to exchange broadening as mentioned above. Overall, the tungstate perturbation of chemical shifts in N74A is similar to that of the WT with some notable exceptions (green circles in Figure 2) in the AL, VI, and Q-loop.

Millisecond Motions in WT and N74A. A comparison of the dynamic behavior between WT VHR and N74A was investigated by solution NMR measurement of the chemical exchange rate constant (R_{ex}) using the TROSY-based Hahn-echo experiment. The experiment was conducted on both the apo and tungstate-bound forms of the WT enzyme and for the tungstate-bound complex of N74A, which was necessary because of excessive exchange broadening in the apo form of this mutant (Figure 4). The 10% trimmed mean of the collective R_{ex} values for all of the enzymes is 0.33 ± 2.12 s^{-1}. R_{ex} values more than two standard deviations (2σ = 4.57 s^{-1}) above this mean are considered indicative of enhanced flexibility relative to the residues with measured R_{ex} values below this threshold (Figure 4). In apo WT, the following residues have R_{ex} values of >4.57 s^{-1}: 6.7 ± 2.7 s^{-1} for R36, 9.8 ± 1.0 for s^{-1} A63, 12.9 ± 2.6 s^{-1} for R66, 24.6 ± 3.6 s^{-1} for N72, 4.7 ± 0.6 s^{-1} for Y78, 9.2 ± 0.6 s^{-1} for K89, 10.7 ± 1.6 s^{-1} for D92, 24.5 ± 2.2 s^{-1} for E95, 10.0 ± 2.5 s^{-1} for F96, 15.1 ± 1.5 s^{-1} for L98, 4.9 ± 1.4 s^{-1} for R119, 4.6 ± 1.4 s^{-1} for C124, 5.7 ± 1.1 s^{-1} for G161, and 5.5 ± 0.6 s^{-1} for D164. These residues comprise the active-site acid loop, the VI loop, and a second previously identified[27] allosteric site α7, containing residues G161 and D164. Eight of these 14 residues were also identified as flexible in the relaxation-compensated CPMG experiment of the WT apoenzyme described above. The R_{ex} values for these eight residues (A63, R66, N72, K89, D92, E95, F96, and L98) are within error of the R_{ex} values determined from the CPMG relaxation dispersion experiment (with the exception of D92) and further verify the consistency between the two measurements. A table of the measured R_{ex} values for each enzyme in the apo and tungstate-bound forms is provided in Table S1.

The profile of flexible residues of the tungstate-bound WT VHR is very similar to that of the apo form, yet with slightly elevated R_{ex} values for some residues. Nearly half of residues with high R_{ex} values in the bound form are in the active site, the recognition loop, and α7. Residues with elevated R_{ex} values in the tungstate complexed form include N13, G19, A62, G65, R66, N72, T73, N74, K89, A90, T93, Q94, E95, F96, N97, S99, Y101, R158, G161, D164, A168, and Q169. The underlined residues can be spectroscopically observed only in the presence of saturating tungstate. Overall, the increase in the number of flexible residues in tungstate-bound WT versus the apo form is likely the result of additional residues becoming spectroscopically observable in the presence of tungstate. These results highlight the allostery present among VI, the α4−α7 region, and the active site and indicate how the effects of ligand binding are propagated to distal regions of the enzyme.

The tungstate-bound N74A complex has R_{ex} values similar to those of WT, such as residues in and near VI, the acid loop, and α7 (T73, G161, N163, D164, G165, and F166), with a few exceptions. Residues G19 (recognition region), T34 (β1), G40 (β2), N41 (α2), A45 (α2), C124 (P-loop), and L134 (α5) show significant flexibility. In WT, R_{ex} values for C124, G165, and F166 could not be quantitated. It is also worth noting that most of the residues in the VI and acid loop in N74A remain exchange-broadened, and thus, the R_{ex} values could not be quantitated. Therefore, while these residues clearly retain or exceed WT-like millisecond motions, a direct comparison is not possible.

For the residues in both WT and N74A enzymes in which R_{ex} values could be determined, the R_{ex} values for those in N74A are within error of the WT value or slightly greater (Figure 4D). Notably, N41, A45, T73, N163, and D164 all have R_{ex} values higher than that of the WT. These enhancements in R_{ex} are an indicator of an increased level of conformational motion in N74A. Under the experimental conditions, considering the measured K_d for tungstate, and estimations of its dissociation rate constant, these elevated R_{ex} values are not due to exchange of WO_4^{2-} on and off of the enzyme, but rather real conformational exchange motions. A summary of residues with millisecond motions in each complex is shown in a Venn diagram in Figure 4E.

VHR Catalytic Activity. To determine the effects of these allosteric mutations on VHR catalytic activity, we measured steady-state and pre-steady-state kinetics for WT, N74A, and K50A using the pseudosubstrate pNPP. K50A was used as a control because it is located near the VI, yet its chemical shift is unperturbed in all of the acid loop mutants examined to date,[27] suggesting the absence of allosteric linkage to the active site. Moreover, the chemical shift of K50 is unperturbed in the presence of either phosphate or tungstate relative to the apoenzyme. Thus, we anticipate that the catalytic activity of K50A will be WT-like and that any differences from WT will be the result of experimental variability and provide an estimate of our measurement precision. The results of the steady-state kinetic assay reveal that K50A has the same kinetic parameters (k_{cat} = 4.3 ± 0.3 s^{-1}, and K_m = 2.1 ± 0.4 mM) as WT VHR (k_{cat} = 4.6 ± 0.1 s^{-1}, and K_m = 2.0 ± 0.1 mM) as seen in Table 1 and Figure S1A. On the basis of these data, we estimate the experimental variability in steady-state kinetic measurement is between 5% and 7% for K_m and k_{cat}. The N74A enzyme has both a slight (21%) decrease in k_{cat} (3.4 ± 0.3 s^{-1}) and a >2-fold increase in K_m (4.7 ± 1.1 mM) compared to those of WT and is outside the experimental "noise" region defined above using K50A as a negative control.

Table 1. Results of the Steady-State (k_{cat} and K_m) and Rapid Kinetics of WT VHR, K50A, and N74A

enzyme	k_{cat} (s^{-1})	K_m (mM)	k_{cleav} (s^{-1})	k_{hydr} (s^{-1})
WT	4.6 ± 0.1	2.0 ± 0.1	19 ± 3	3.3 ± 0.1
K50A	4.3 ± 0.3	2.1 ± 0.4	22 ± 2	3.1 ± 0.2
N74A	3.4 ± 0.3	4.7 ± 1.1	7.9 ± 0.8	1.17 ± 0.03

https://dx.doi.org/10.1021/acs.biochem.0c00245
Biochemistry 2020, 59, 1896−1908

Thus, this allosteric mutant affects both the catalytic and substrate binding steps. To ascertain the effects of mutation on the individual reaction steps, we measured the cleavage and hydrolysis rates using stopped-flow kinetic experiments.

The reported rate constant for cleavage of pNPP by VHR ($k_{cleavage}$ = 34 s^{-1}) is ∼4 times faster than the rate of the hydrolysis step (7.6 s^{-1}) at 30 °C.[46] Our experiments were performed on WT VHR, K50A, and N74A at 25 °C on the same day in an effort to minimize experimental variation. The kinetic traces and fits with eq 1 are shown in Figure S1B, and the results are listed in Table 1. At 25 °C for WT VHR, the measured cleavage rate constants $k_{cleavage}$ = 19 ± 3 s^{-1} and $k_{hydrolysis}$ = 3.3 ± 0.1 s^{-1}. These values are slightly lower than the reported literature values most likely due to the lower temperature at which our experiments were conducted.[46] The control enzyme, K50A, has a $k_{cleavage}$ of 22 ± 2 s^{-1} and a $k_{hydrolysis}$ of 3.2 ± 0.2 s^{-1}, values very similar to those for the WT. The N74A mutant has a significant impact on both $k_{cleavage}$ and $k_{hydrolysis}$ compared to those of the WT, where these values are 7.9 and 1.2 s^{-1}, respectively, a roughly 2-fold decrease for both kinetic parameters.

Computational Analysis of VHR. Molecular dynamics simulations for the tungstate-bound forms of WT, N74A, and K50A VHR enzymes provide valuable mechanistic insights. First, for WT and K50A, the simulations reveal that the acid loop moves from its starting closed position to an open conformation, further hinting at WT VHR having a flexible acid loop. A global comparison between WT, N74A, and K50A reveals very similar structures during the 150 ns simulations, with the root-mean-square deviation (RMSD) of the C_α atoms between these enzymes being 0.642 Å (WT vs N74A) and 0.796 Å (WT vs K50A), indicating that neither mutation causes a large overall structural change. However, the N74A mutation produces significant changes in hydrogen bonding that affect the opening of the acid loop and the positioning of the tungstate ligand. Indeed, a close examination of selected regions of VHR reveals critical changes caused by the mutation at N74. Figure 5 shows that the side chain of R125 in the P-loop is displaced and becomes more rigid in the N74A mutant. Its displacement shifts the neighboring E126 away from the active site, where it would otherwise repel the side chain of D92 and open the acid loop. The resulting changes in the acid loop motion correlate with a decrease in catalytic activity, which could result from suppression of substrate entry, or product exit, from the active site, or a disruption in the timing of events necessary for optimal VHR catalysis.

Overall, the acid loop RMSF shown in Figure 5 reveals a large difference between WT and N74A, which is due to the acid loop remaining closed in the mutant. This is despite a distance of almost 20 Å between N74 and the active site. However, Figure 5 shows the path of perturbations that start at the mutation and lead to the locking of the acid loop in the closed position. The N74A mutation causes an unraveling of the short helix in the VI region comprising residues 74−78, which distorts the remainder of the VI loop. Figure 6 shows the hydrogen bonding changes that begin with N72 being pulled out of its hydrogen bonds with other residues in the VI loop to replace A74 as a solvent-exposed residue. This changes the orientation of the backbone of neighboring H70 just enough to form a stronger hydrogen bond with R125. With the R125 side chain pulled to the side, E126 is also displaced. In WT and K50A, E126 and D92 jockey for space at the active site. Repulsion between them allows for the breakage of the

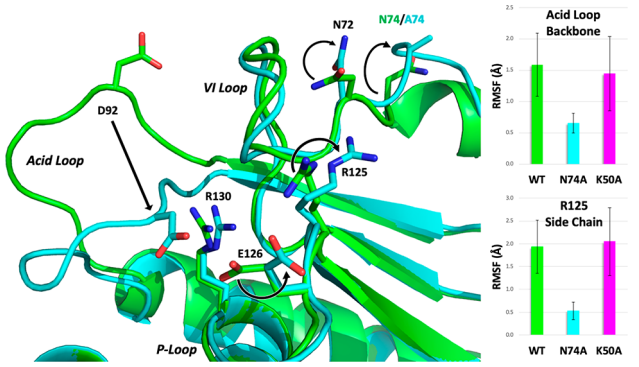

Figure 5. Structural differences revealed by the MD simulations of WT (green), K50A (magenta), and N74A (cyan) bound to tungstate (not shown). The right panel shows the root-mean-square fluctuations (RMSF) for the acid loop and side chain of R125 for the latter 100 ns of the simulation, highlighting the differences in flexibility between WT/K50A and N74A. The side chain of R125 becomes more rigid in the N74A mutant (smaller RMSF). Its displacement shifts E126 away from the active site, consequently suppressing the electrostatic repulsion with D92, essential for opening of the acid loop (smaller RMSF). The resulting changes in the acid loop motion correlate with a decrease in catalytic activity, which could result from the suppression of substrate entry or product exit from the active site.

hydrogen bond between R130 and the A90 backbone, which holds the acid loop closed. E126 also serves as a cap on the active site, keeping the opening small even when the loop is open (Figure 7). In N74A, E126 is less sterically hindered by R125 and is more willing to yield the active site to D92.

The resulting structural changes prevent the N74A acid loop from opening, leaving D92 separated by 5Å in the mutant when compared to its configuration in the WT. The acid loop in both WT and K50A can open fairly easily while the loop remains firmly closed in N74A (Figure 5). The flexibility of the acid loop in WT and K50A increases the loop's RMSF over the final 100 ns of the simulation from 0.656 Å (N74A) to ∼1.5 Å (WT and K50A) and the global backbone RMSF from 0.789 Å (N74A) to almost 1 Å in both WT and K50A. Moreover, these differences in WT and K50A result in the tungstate molecule moving farther into the active site by ∼1.4 Å, as compared to that in N74A. Predictably, this movement changes the hydrogen bonding partners of tungstate. As shown in Figure 6, the tungstate of WT shares strong hydrogen bonds with R125, E126, R130, and S131. The more raised location in N74A forms much stronger hydrogen bonds with R130 and favors Y128 and S129 over R125 and E126. The alteration of the position of the catalytic acid and the change in location of the product analogue relative to its WT structure are likely responsible for the diminished catalytic activity of the N74A enzyme.

Given the alterations in loop flexibility observed both experimentally and computationally, we compared the chemical shift differences, $\Delta\omega$, determined by NMR relaxation dispersion studies of apo WT VHR, with $\Delta\delta$ chemical shift changes as a result of tungstate titration for WT VHR. Previously, correspondence between these values has been taken as evidence that the apoenzyme naturally samples the bound conformation in the absence of a ligand.[66−68] The comparison for VHR is shown in Figure 8. The data in Figure 8 show that for all residues for which a measurement could be

https://dx.doi.org/10.1021/acs.biochem.0c00245
Biochemistry 2020, 59, 1896−1908

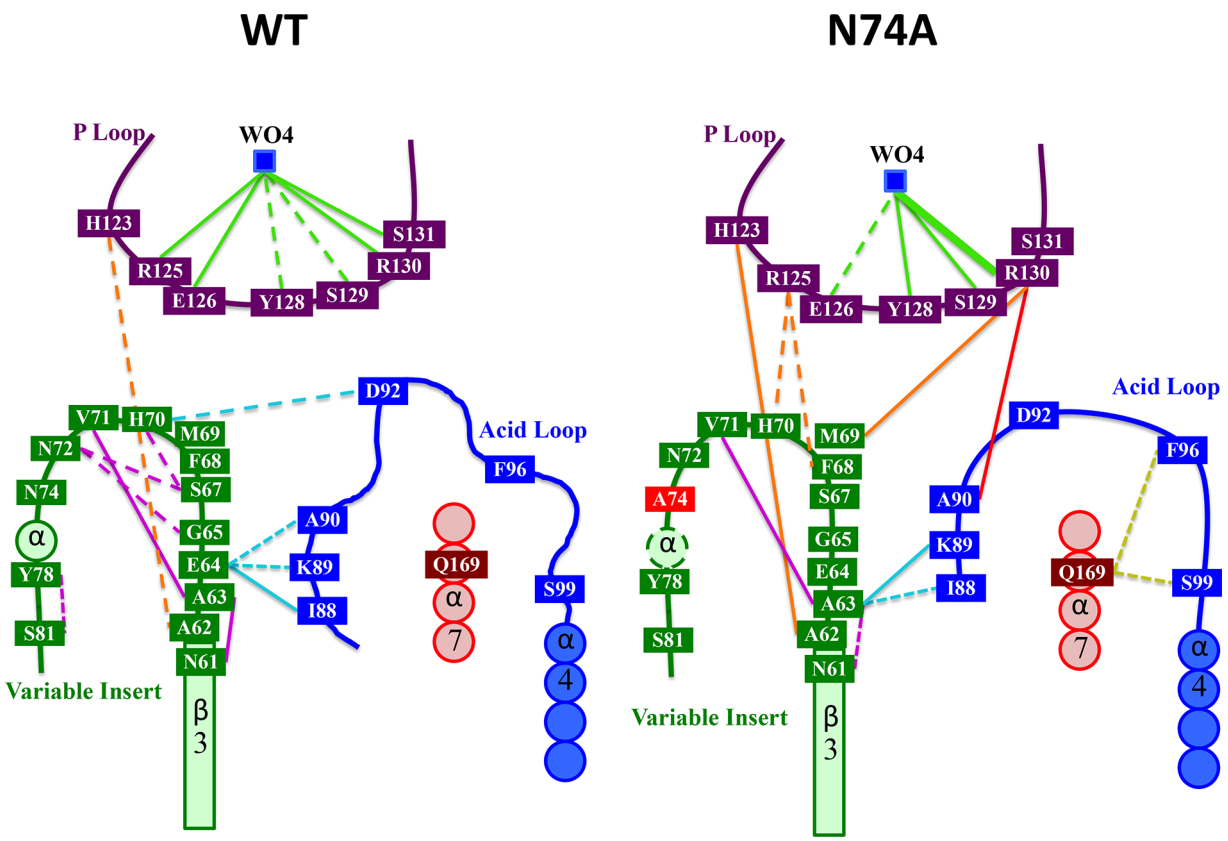

Figure 6. Summary of the effects of the N74A mutation. Lines indicate H-bonds observed for 33−66% (dotted), >66% (solid), and 100% (thick solid) of the entire MD trajectory.

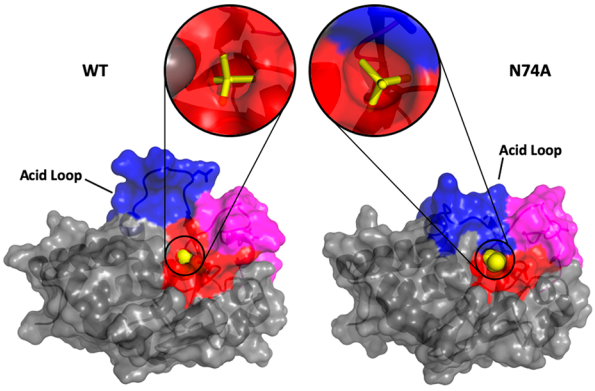

Figure 7. Surface rendering of the WT (left) and the N74A mutant (right) for a representative configuration of the MD simulation. The acid loop is colored blue, the VI loop magenta, and the P-loop red. The close-up view depicts WO_4^{2-} (yellow) bound at the active site. The surfaces shown in the bottom panel highlight that for the WT enzyme, the acid loop is more open, alhtough the WO_4^{2-} molecule is more buried than in N74A, due to differences in hydrogen bonding.

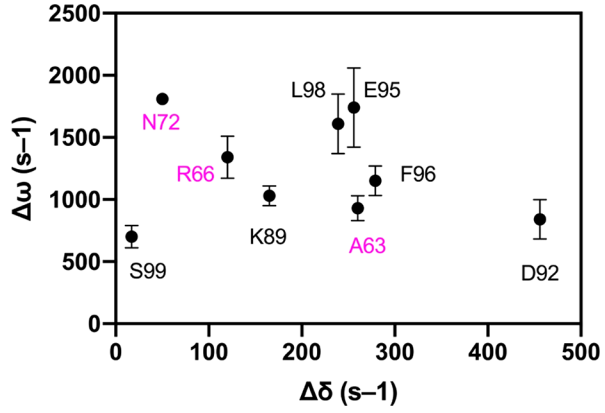

Figure 8. Chemical shift differences. Dynamic chemical shift changes ($\Delta\omega$) in apo VHR from CPMG relaxation dispersion experiments plotted vs chemical shift changes ($\Delta\delta$) from a tungstate titration into apo VHR. Residues are labeled and colored with VI residues in magenta and acid loop residues in black. The lack of correlation between the two values indicates that loop motions in the apoenzyme are distinct from those conformational changes that occur due to ligand binding.

taken $\Delta\omega$ values for loop residues are significantly larger than $\Delta\delta$ values for the same residues.

DISCUSSION

The allosteric linkage between the variable insert region and the acid loop in VHR was originally verified when alanine scanning mutations of the acid loop resulted in chemical shift perturbations for residues located in the VI loop.[27] The work presented here expands on those studies by showing that the enzymatic reaction product (inorganic phosphate) and product analogue (tungstate) alter the chemical shifts not only at the active site but also for residues located in VI, including N74. Furthermore, NMR CPMG relaxation dispersion experiments indicate that the acid loop and VI are flexible on the millisecond time scale. In addition, the identical exchange rate constant and equilibrium populations that describe this motion suggest that the VI and acid loop motions are coupled. The implication of these data is that alterations to the VI

https://dx.doi.org/10.1021/acs.biochem.0c00245
Biochemistry 2020, 59, 1896−1908

should affect enzyme function, which we have observed in this work via steady- and pre-steady-state kinetics for the N74A mutation showing that this mutation alters both chemistry steps and steady-state substrate binding. Interestingly, it has been previously shown using unnatural amino acid incorporation at the VI residue F68 that VI can be a site for VHR dimerization and that this interaction inhibits enzyme activity.[44] Wu et al. also showed that VI residues F68 and M69 as well as residues in the substrate recognition loop contribute to the binding of the inhibitor, SA3.[43] Cumulatively, these data indicate that alterations to the VI sequence can disrupt VHR function and that residues in the VI could provide a binding platform for small molecule inhibitors. It further seems reasonable to speculate that *in vivo*, Nature may utilize the VI as a structural feature that is recognized by other protein regulators or substrates. For example, the pseudokinase VRK3 binds to VHR and inhibits its catalytic activity.[69] Although the binding interface between VRK3 and VHR is not known, these studies here suggest that VI represents a potential starting point to identify such an interaction.

Molecular Motions in WT VHR. To investigate the mechanism of the interaction between the VI and acid loop that results in altered enzyme function, we performed 150 ns molecular dynamics simulations for WT, K50A, and N74A all with tungstate bound to the active-site P-loop. WT and K50A simulations show very similar behavior, again confirming the innocuous nature of mutation of residue 50. Therefore, the discussion that follows will focus on the WT enzyme and a comparison to N74A. As shown in Figure 6, the linkage between the VI and acid loop is mediated by hydrogen bonds that connect E64 with the N-terminus of the acid loop (A90, K89, and I88). One additional interaction between these two regions in VHR is a hydrogen bond between H70 and the catalytic acid D92. Moreover, within the VI loop itself, there are hydrogen bonds that connect residues in the N-terminal portion of VI with those in the center of the VI. These connections are likely responsible for the identical millisecond motions that are observed for residues in the VI and acid loop. On the faster time scale of the nanosecond simulations, the WT interactions between the VI and acid loop lead to an opening of the acid loop (Figure 7A).

Molecular Motions in N74A VHR. In contrast, in N74A, the unraveling of the short helical region around residue 74 in VI is propagated to the acid loop and active site in such a way that weakens the hydrogen bonding between the VI and acid loop as well as the intra-VI hydrogen bonds (Figure 6). Moreover, new H-bonds are now formed between VI and Q169 in α7 and between the acid loop and the P-loop of N74A (Figure 6). This rearrangement of hydrogen bonds results in a rigidification of the acid loop and a conformation that remains closed. In addition, new H-bonds are formed between the acid loop and the P-loop and between the VI and P-loop, which were not observed in the simulations of the WT. These new interactions result in additional closing of the acid loop and a reduction of the WT-like interface around the active site, possibly limiting interaction with the substrate (Figure 7B). An assessment of the flexibility of the active site in the acid and P-loops (Figure 5) shows that the fluctuations of the acid loop are decreased in N74A as well as in the P-loop side chain R125. Thus, this allosteric mutation makes R125 and consequently the acid loop more rigid, likely weakening hydrogen bonds that stabilize the substrate at the active site. The allostery in VHR causes the VI loop to twist upon changes at residue 74, which gives R125 in the P-loop better access to the backbone of H70 in VI. With R125 pulled to the side by a hydrogen bond, E126 can also move to one side, weakening its interaction with D92 and the substrate. Without this interaction, tungstate is not pushed down into the pocket and the acid loop loses flexibility. The functional result of this mutation is a disruption in the picosecond to nanosecond motion of the acid loop, a displacement of the catalytic acid D92, inefficient phosphoryl cleavage, and a change in the binding mode for the anionic portion of the substrate.

The results presented here are to be contrasted with the view of the VHR acid loop as being rigid in the WT enzyme. As noted in the introductory section, this current view is mainly due to the absence of an observed structure of VHR with an open acid loop conformation. In fairness, there is no true "apo" structure of VHR as all three structures in the PDB have some variant of an anion bound to the P-loop and the acid loop is in the closed conformation in these structures. The CPMG dispersion and Hahn-echo NMR results here conclusively establish that the apo acid loop is moving on the millisecond time scale. In the tungstate-bound form of VHR, these motions remain as shown by the Hahn-echo experiment. In addition, the computational studies show significant backbone motions during the faster time scale of the MD simulations. Thus, it would appear that VHR has a flexible acid loop like other members of the PTP family such as YopH and PTP1B.

However, in YopH and PTP1B,[68] the NMR data suggested that the apoenzyme acid loop transiently sampled the closed conformation and conversely, when bound to the substrate analogue, the acid loop was predominantly closed yet sampled the open acid loop conformation. This conclusion was based on the similarity of chemical shift differences for loop residues between the open and closed conformation ($|\Delta\delta_N|$) with the dynamic chemical shift differences ($|\Delta\omega_N|$) determined by CPMG relaxation dispersion experiments. The agreement between these values seen in those enzymes is not observed for VHR (Figure 8). The $|\Delta\omega_N|$ values of the acid loop residues from CPMG dispersion experiments are 1030, 840, 1740, 1150, 1610, and 700 s^{-1} for K89, D92, E95, F96, L98, and S99, respectively. These values are much greater than the $|\Delta\delta_N|$ from the tungstate titrations, which are 165, 456, 256, 279, 239, and 17 s^{-1} for the same residues. The same trend is true for the VI residues in which $|\Delta\omega_N|$ values from the CPMG dispersion experiments are 930, 1340, and 1810 s^{-1} compared to $|\Delta\delta_N|$ values of 260, 120, and 50 s^{-1} for A63, R66, and N72, respectively, from the tungstate titrations suggesting that the innate conformational motions in the apo WT are different from the conformational changes as a result of ligand binding and the structures that are interconverting in VHR on the millisecond time scale remain unclear and represent an obvious next step in the studies of this enzyme.

CONCLUSION

Although all of the details of the molecular motions of the acid loop and VI in VHR remain to be determined, the changes in motions, chemical shifts, and enzyme activity between WT and N74A suggest their importance in its dephosphorylation activity. There is an intimate connection between the acid loop and VI in VHR that is important to the binding and cleavage of the substrate. Disruptions at residue 74 change the hydrogen bonding pattern and are propagated to the acid loop and P-loop. These changes affect the motions critical to the

https://dx.doi.org/10.1021/acs.biochem.0c00245
Biochemistry 2020, 59, 1896−1908

mechanism and cause inefficient binding and catalytic activity. The link between the VI and the acid loop in VHR may illuminate mechanisms of *in vivo* regulation and may also represent an avenue toward drugging VHR with small molecule ligands. Furthermore, in a recent study of 30 dual-specificity PTP enzymes, a majority of acid loops in these enzymes have been demonstrated to be closed, with a few showing open loops.[70] However, like VHR, all contained a negatively charged molecule at the acid site. Given the similarities between those enzymes and VHR, it seems possible that these enzymes also possess mobile acid loops, which could lend themselves to allosteric targeting via their variable insert regions.

■ ASSOCIATED CONTENT

Supporting Information

The Supporting Information is available free of charge at https://pubs.acs.org/doi/10.1021/acs.biochem.0c00245.

A table listing R_{ex} values for WT VHR and mutant enzymes along with figures containing enzyme kinetic data and 2D NMR $^{1}H-^{15}N$ HSQC spectra (PDF)

Accession Codes

The UniProt accession code for human *Vaccinia* H1-related phosphatase is 541452.

■ AUTHOR INFORMATION

Corresponding Authors

Victor S. Batista − *Department of Chemistry, Yale University, New Haven, Connecticut 06520, United States;* orcid.org/0000-0002-3262-1237; Email: Victor.Batista@yale.edu

J. Patrick Loria − *Department of Chemistry and Department of Molecular Biophysics and Biochemistry, Yale University, New Haven, Connecticut 06520, United States;* orcid.org/0000-0002-4824-9089; Email: Patrick.loria@yale.edu

Authors

Victor A. Beaumont − *Department of Chemistry, Yale University, New Haven, Connecticut 06520, United States*

Krystle Reiss − *Department of Chemistry, Yale University, New Haven, Connecticut 06520, United States*

Zexing Qu − *Department of Chemistry, Yale University, New Haven, Connecticut 06520, United States; Institute for Theoretical Chemistry, Jilin University, Changchun 130023, China*

Brandon Allen − *Department of Chemistry, Yale University, New Haven, Connecticut 06520, United States*

Complete contact information is available at: https://pubs.acs.org/10.1021/acs.biochem.0c00245

Funding

V.A.B. and K.R. acknowledge support from National Institutes of Health Biophysics Training Grant T32 GM008283. J.P.L. and V.B. acknowledge Grant GM121781. J.P.L. acknowledges Grant MCB 1615415. V.S.B. acknowledges Grant GM106121 and supercomputer resources from NSERSC.

Notes

The authors declare no competing financial interest.

■ REFERENCES

(1) Alonso, A., Sasin, J., Bottini, N., Friedberg, I., Friedberg, I., Osterman, A., Godzik, A., Hunter, T., Dixon, J., and Mustelin, T. (2004) Protein tyrosine phosphatases in the human genome. *Cell 117*, 699−711.

(2) Barr, A. J. (2010) Protein tyrosine phosphatases as drug targets: strategies and challenges of inhibitor development. *Future Med. Chem. 2*, 1563−1576.

(3) Tautz, L., Critton, D. A., and Grotegut, S. (2013) Protein tyrosine phosphatases: structure, function, and implication in human disease. *Methods Mol. Biol. 1053*, 179−221.

(4) Tonks, N. K. (2006) Protein tyrosine phosphatases: from genes, to function, to disease. *Nat. Rev. Mol. Cell Biol. 7*, 833−846.

(5) Todd, J. L., Tanner, K. G., and Denu, J. M. (1999) Extracellular regulated kinases (ERK) 1 and ERK2 are authentic substrates for the dual-specificity protein-tyrosine phosphatase VHR. A novel role in down-regulating the ERK pathway. *J. Biol. Chem. 274*, 13271−13280.

(6) Yuvaniyama, J., Denu, J. M., Dixon, J. E., and Saper, M. A. (1996) Crystal structure of the dual specificity protein phosphatase VHR. *Science 272*, 1328−1331.

(7) Hoyt, R., Zhu, W., Cerignoli, F., Alonso, A., Mustelin, T., and David, M. (2007) Cutting edge: selective tyrosine dephosphorylation of interferon-activated nuclear STAT5 by the VHR phosphatase. *J. Immunol. 179*, 3402−3406.

(8) Todd, J. L., Rigas, J. D., Rafty, L. A., and Denu, J. M. (2002) Dual-specificity protein tyrosine phosphatase VHR down-regulates c-Jun N-terminal kinase (JNK). *Oncogene 21*, 2573−2583.

(9) Wang, J. Y., Yeh, C. L., Chou, H. C., Yang, C. H., Fu, Y. N., Chen, Y. T., Cheng, H. W., Huang, C. Y., Liu, H. P., Huang, S. F., and Chen, Y. R. (2011) Vaccinia H1-related phosphatase is a phosphatase of ErbB receptors and is down-regulated in non-small cell lung cancer. *J. Biol. Chem. 286*, 10177−10184.

(10) Henkens, R., Delvenne, P., Arafa, M., Moutschen, M., Zeddou, M., Tautz, L., Boniver, J., Mustelin, T., and Rahmouni, S. (2008) Cervix carcinoma is associated with an up-regulation and nuclear localization of the dual-specificity protein phosphatase VHR. *BMC Cancer 8*, 147.

(11) Ishibashi, T., Bottaro, D. P., Chan, A., Miki, T., and Aaronson, S. A. (1992) Expression cloning of a human dual-specificity phosphatase. *Proc. Natl. Acad. Sci. U. S. A. 89*, 12170−12174.

(12) Rahmouni, S., Cerignoli, F., Alonso, A., Tsutji, T., Henkens, R., Zhu, C., Louis-dit-Sully, C., Moutschen, M., Jiang, W., and Mustelin, T. (2006) Loss of the VHR dual-specific phosphatase causes cell-cycle arrest and senescence. *Nat. Cell Biol. 8*, 524−531.

(13) Hao, L., and ElShamy, W. M. (2007) BRCA1-IRIS activates cyclin D1 expression in breast cancer cells by downregulating the JNK phosphatase DUSP3/VHR. *Int. J. Cancer 121*, 39−46.

(14) Zhang, Z. Y. (2017) Drugging the Undruggable: Therapeutic Potential of Targeting Protein Tyrosine Phosphatases. *Acc. Chem. Res. 50*, 122−129.

(15) Stanford, S. M., and Bottini, N. (2017) Targeting Tyrosine Phosphatases: Time to End the Stigma. *Trends Pharmacol. Sci. 38*, 524−540.

(16) De Amici, M., Dallanoce, C., Holzgrabe, U., Trankle, C., and Mohr, K. (2009) Allosteric Ligands for G Protein-Coupled Receptors: A Novel Strategy with Attractive Therapeutic Opportunities. *Med. Res. Rev. 30*, 463−549.

(17) Kanuma, K., Aoki, T., and Shimazaki, Y. (2010) Recent patents on positive allosteric modulators of the metabotropic glutamate 5 receptor as a potential treatment for schizophrenia. *Recent Pat. CNS Drug Discovery 5*, 23−34.

(18) Scheuermann, T. H., Li, Q., Ma, H. W., Key, J., Zhang, L., Chen, R., Garcia, J. A., Naidoo, J., Longgood, J., Frantz, D. E., Tambar, U. K., Gardner, K. H., and Bruick, R. K. (2013) Allosteric inhibition of hypoxia inducible factor-2 with small molecules. *Nat. Chem. Biol. 9*, 271−276.

(19) Jin, L., and Harrison, S. C. (2002) Crystal structure of human calcineurin complexed with cyclosporin A and human cyclophilin. *Proc. Natl. Acad. Sci. U. S. A. 99*, 13522−13526.

(20) Kissinger, C. R., Parge, H. E., Knighton, D. R., Lewis, C. T., Pelletier, L. A., Tempczyk, A., Kalish, V. J., Tucker, K. D., Showalter, R. E., Moomaw, E. W., et al. (1995) Crystal structures of human

calcineurin and the human FKBP12-FK506-calcineurin complex. *Nature 378*, 641−644.
(21) Krishnan, N., Koveal, D., Miller, D. H., Xue, B., Akshinthala, S. D., Kragelj, J., Jensen, M. R., Gauss, C. M., Page, R., Blackledge, M., Muthuswamy, S. K., Peti, W., and Tonks, N. K. (2014) Targeting the disordered C terminus of PTP1B with an allosteric inhibitor. *Nat. Chem. Biol. 10*, 558−566.
(22) Wiesmann, C., Barr, K. J., Kung, J., Zhu, J., Erlanson, D. A., Shen, W., Fahr, B. J., Zhong, M., Taylor, L., Randal, M., McDowell, R. S., and Hansen, S. K. (2004) Allosteric inhibition of protein tyrosine phosphatase 1B. *Nat. Struct. Mol. Biol. 11*, 730−737.
(23) Peti, W., and Page, R. (2015) Strategies to make protein serine/threonine (PP1, calcineurin) and tyrosine phosphatases (PTP1B) druggable: achieving specificity by targeting substrate and regulatory protein interaction sites. *Bioorg. Med. Chem. 23*, 2781−2785.
(24) Wang, X., Bajaj, R., Bollen, M., Peti, W., and Page, R. (2016) Expanding the PP2A Interactome by Defining a B56-Specific SLiM. *Structure 24*, 2174−2181.
(25) Petit, C. M., Zhang, J., Sapienza, P. J., Fuentes, E. J., and Lee, A. L. (2009) Hidden dynamic allostery in a PDZ domain. *Proc. Natl. Acad. Sci. U. S. A. 106*, 18249−18254.
(26) Zhang, J., Sapienza, P. J., Ke, H., Chang, A., Hengel, S. R., Wang, H., Phillips, G. N., and Lee, A. L. (2010) Crystallographic and nuclear magnetic resonance evaluation of the impact of peptide binding to the second PDZ domain of protein tyrosine phosphatase 1E. *Biochemistry 49*, 9280−9291.
(27) Cui, D. S., Beaumont, V., Ginther, P. S., Lipchock, J. M., and Loria, J. P. (2017) Leveraging Reciprocity to Identify and Characterize Unknown Allosteric Sites in Protein Tyrosine Phosphatases. *J. Mol. Biol. 429*, 2360−2372.
(28) Abdel-Magid, A. F. (2015) Allosteric modulators: an emerging concept in drug discovery. *ACS Med. Chem. Lett. 6*, 104−107.
(29) Abdel-Magid, A. F. (2017) Therapeutic Advantage of the Positive Allosteric Modulators of the GABA-B Receptor. *ACS Med. Chem. Lett. 8*, 474−475.
(30) Vagnarelli, P., and Alessi, D. R. (2018) PP1 Phosphatase Complexes: Undruggable No Longer. *Cell 174*, 1049−1051.
(31) Grzyska, P. K., Kim, Y., Jackson, M. D., Hengge, A. C., and Denu, J. M. (2004) Probing the transition-state structure of dual-specificity protein phosphatases using a physiological substrate mimic. *Biochemistry 43*, 8807−8814.
(32) Hengge, A. C., Denu, J. M., and Dixon, J. E. (1996) Transition-state structures for the native dual-specific phosphatase VHR and D92N and S131A mutants. Contributions to the driving force for catalysis. *Biochemistry 35*, 7084−7092.
(33) Denu, J. M., and Dixon, J. E. (1995) A catalytic mechanism for the dual-specific phosphatases. *Proc. Natl. Acad. Sci. U. S. A. 92*, 5910−5914.
(34) Brandao, T. A., Robinson, H., Johnson, S. J., and Hengge, A. C. (2009) Impaired acid catalysis by mutation of a protein loop hinge residue in a YopH mutant revealed by crystal structures. *J. Am. Chem. Soc. 131*, 778−786.
(35) Rigas, J. D., Hoff, R. H., Rice, A. E., Hengge, A. C., and Denu, J. M. (2001) Transition state analysis and requirement of Asp-262 general acid/base catalyst for full activation of dual-specificity phosphatase MKP3 by extracellular regulated kinase. *Biochemistry 40*, 4398−4406.
(36) Pavic, K., Duan, G., and Kohn, M. (2015) VHR/DUSP3 phosphatase: structure, function and regulation. *FEBS J. 282*, 1871−1890.
(37) Brandao, T. A., Hengge, A. C., and Johnson, S. J. (2010) Insights into the reaction of protein-tyrosine phosphatase 1B: crystal structures for transition state analogs of both catalytic steps. *J. Biol. Chem. 285*, 15874−15883.
(38) Brandao, T. A., Johnson, S. J., and Hengge, A. C. (2012) The molecular details of WPD-loop movement differ in the protein-tyrosine phosphatases YopH and PTP1B. *Arch. Biochem. Biophys. 525*, 53−59.
(39) Barford, D., Flint, A. J., and Tonks, N. K. (1994) Crystal structure of human protein tyrosine phosphatase 1B. *Science 263*, 1397−1404.
(40) Denu, J. M., Lohse, D. L., Vijayalakshmi, J., Saper, M. A., and Dixon, J. E. (1996) Visualization of intermediate and transition-state structures in protein-tyrosine phosphatase catalysis. *Proc. Natl. Acad. Sci. U. S. A. 93*, 2493−2498.
(41) Phan, J., Lee, K., Cherry, S., Tropea, J. E., Burke, T. R., Jr., and Waugh, D. S. (2003) High-resolution structure of the Yersinia pestis protein tyrosine phosphatase YopH in complex with a phosphotyrosyl mimetic-containing hexapeptide. *Biochemistry 42*, 13113−13121.
(42) Schumacher, M. A., Todd, J. L., Rice, A. E., Tanner, K. G., and Denu, J. M. (2002) Structural basis for the recognition of a bisphosphorylated MAP kinase peptide by human VHR protein Phosphatase. *Biochemistry 41*, 3009−3017.
(43) Wu, S., Vossius, S., Rahmouni, S., Miletic, A. V., Vang, T., Vazquez-Rodriguez, J., Cerignoli, F., Arimura, Y., Williams, S., Hayes, T., Moutschen, M., Vasile, S., Pellecchia, M., Mustelin, T., and Tautz, L. (2009) Multidentate small-molecule inhibitors of vaccinia H1-related (VHR) phosphatase decrease proliferation of cervix cancer cells. *J. Med. Chem. 52*, 6716−6723.
(44) Pavic, K., Rios, P., Dzeyk, K., Koehler, C., Lemke, E. A., and Kohn, M. (2014) Unnatural amino acid mutagenesis reveals dimerization as a negative regulatory mechanism of VHR's phosphatase activity. *ACS Chem. Biol. 9*, 1451−1459.
(45) Bellstedt, P., Seiboth, T., Hafner, S., Kutscha, H., Ramachandran, R., and Gorlach, M. (2013) Resonance assignment for a particularly challenging protein based on systematic unlabeling of amino acids to complement incomplete NMR data sets. *J. Biomol. NMR 57*, 65−72.
(46) Zhang, Z. Y., Wu, L., and Chen, L. (1995) Transition state and rate-limiting step of the reaction catalyzed by the human dual-specificity phosphatase, VHR. *Biochemistry 34*, 16088−16096.
(47) Lee, W., Tonelli, M., and Markley, J. L. (2015) NMRFAM-SPARKY: enhanced software for biomolecular NMR spectroscopy. *Bioinformatics 31*, 1325−1327.
(48) Keller, R. (2004) The computer aided resonance assignment tutorial (CANTINA). Verlag. http://www.cara.nmr-software.org/.
(49) Grzesiek, S., Stahl, S. J., Wingfield, P. T., and Bax, A. (1996) The CD4 determinant for downregulation by HIV-1 Nef directly binds to Nef. Mapping of the Nef binding surface by NMR. *Biochemistry 35*, 10256−10261.
(50) Loria, J. P., Rance, M., and Palmer, A. G. (1999) A relaxation-compensated Carr-Purcell-Meiboom-Gill sequence for characterizing chemical exchange by NMR spectroscopy. *J. Am. Chem. Soc. 121*, 2331−2332.
(51) Mulder, F. A., Skrynnikov, N. R., Hon, B., Dahlquist, F. W., and Kay, L. E. (2001) Measurement of slow (micros-ms) time scale dynamics in protein side chains by (15)N relaxation dispersion NMR spectroscopy: application to Asn and Gln residues in a cavity mutant of T4 lysozyme. *J. Am. Chem. Soc. 123*, 967−975.
(52) Carver, J. P., and Richards, R. E. (1972) A general two-site solution for the chemical exchange produced dependence of T2 upon the Carr-Purcell pulse separation. *J. Magn. Reson. 6*, 89−105.
(53) Wang, C., Rance, M., and Palmer, A. G., 3rd. (2003) Mapping chemical exchange in proteins with MW > 50 kD. *J. Am. Chem. Soc. 125*, 8968−8969.
(54) Huang, J., and MacKerell, A. D., Jr. (2013) CHARMM36 all-atom additive protein force field: validation based on comparison to NMR data. *J. Comput. Chem. 34*, 2135−2145.
(55) Phillips, J. C., Braun, R., Wang, W., Gumbart, J., Tajkhorshid, E., Villa, E., Chipot, C., Skeel, R. D., Kale, L., and Schulten, K. (2005) Scalable molecular dynamics with NAMD. *J. Comput. Chem. 26*, 1781−1802.
(56) Humphrey, W., Dalke, A., and Schulten, K. (1996) VMD: visual molecular dynamics. *J. Mol. Graphics 14*, 33−38.
(57) Loria, J. P., Rance, M., and Palmer, A. G., 3rd. (1999) Transverse-relaxation-optimized (TROSY) gradient-enhanced triple-resonance NMR spectroscopy. *J. Magn. Reson. 141*, 180−184.

https://dx.doi.org/10.1021/acs.biochem.0c00245
Biochemistry 2020, 59, 1896−1908

(58) Salzmann, M., Wider, G., Pervushin, K., Senn, H., and Wuthrich, K. (1999) TROSY-type triple-resonance experiments for sequential NMR assignments of large proteins. *J. Am. Chem. Soc. 121*, 844−848.
(59) Lee, W., Westler, W. M., Bahrami, A., Eghbalnia, H. R., and Markley, J. L. (2009) PINE-SPARKY: graphical interface for evaluating automated probabilistic peak assignments in protein NMR spectroscopy. *Bioinformatics 25*, 2085−2087.
(60) Selvaratnam, R., Chowdhury, S., VanSchouwen, B., and Melacini, G. (2011) Mapping allostery through the covariance analysis of NMR chemical shifts. *Proc. Natl. Acad. Sci. U. S. A. 108*, 6133−6138.
(61) Khajehpour, M., Wu, L., Liu, S., Zhadin, N., Zhang, Z. Y., and Callender, R. (2007) Loop dynamics and ligand binding kinetics in the reaction catalyzed by the Yersinia protein tyrosine phosphatase. *Biochemistry 46*, 4370−4378.
(62) Schubert, H. L., Fauman, E. B., Stuckey, J. A., Dixon, J. E., and Saper, M. A. (1995) A ligand-induced conformational change in the Yersinia protein tyrosine phosphatase. *Protein Sci. 4*, 1904−1913.
(63) Wang, F., Li, W., Emmett, M. R., Hendrickson, C. L., Marshall, A. G., Zhang, Y. L., Wu, L., and Zhang, Z. Y. (1998) Conformational and dynamic changes of Yersinia protein tyrosine phosphatase induced by ligand binding and active site mutation and revealed by H/D exchange and electrospray ionization Fourier transform ion cyclotron resonance mass spectrometry. *Biochemistry 37*, 15289−15299.
(64) Kuznetsov, V. I., Hengge, A. C., and Johnson, S. J. (2012) New aspects of the phosphatase VHZ revealed by a high-resolution structure with vanadate and substrate screening. *Biochemistry 51*, 9869−9879.
(65) Kovrigin, E. L., Kempf, J. G., Grey, M., and Loria, J. P. (2006) Faithful estimation of dynamics parameters from CPMG relaxation dispersion measurements. *J. Magn. Reson. 180*, 93−104.
(66) Beach, H., Cole, R., Gill, M. L., and Loria, J. P. (2005) Conservation of μs-ms enzyme motions in the apo- and substrate-mimicked state. *J. Am. Chem. Soc. 127*, 9167−9176.
(67) Boehr, D. D., McElheny, D., Dyson, H. J., and Wright, P. E. (2006) The dynamic energy landscape of dihydrofolate reductase catalysis. *Science 313*, 1638−1642.
(68) Whittier, S. K., Hengge, A. C., and Loria, J. P. (2013) Conformational motions regulate phosphoryl transfer in related protein tyrosine phosphatases. *Science 341*, 899−903.
(69) Kang, T. H., and Kim, K. T. (2006) Negative regulation of ERK activity by VRK3-mediated activation of VHR phosphatase. *Nat. Cell Biol. 8*, 863−869.
(70) Jeong, D. G., Wei, C. H., Ku, B., Jeon, T. J., Chien, P. N., Kim, J. K., Park, S. Y., Hwang, H. S., Ryu, S. Y., Park, H., Kim, D. S., Kim, S. J., and Ryu, S. E. (2014) The family-wide structure and function of human dual-specificity protein phosphatases. *Acta Crystallogr., Sect. D: Biol. Crystallogr. 70*, 421−435.

https://dx.doi.org/10.1021/acs.biochem.0c00245
Biochemistry 2020, 59, 1896−1908